Ahmed A. Alkhafaji
Department of Mechanical Engineering,
University of Wisconsin—Milwaukee,
Milwaukee, WI 53211
e-mail: alkhafa2@uwm.edu

Osama M. Selim
Department of Mechanical Engineering,
University of Wisconsin—Milwaukee,
Milwaukee, WI 53211
e-mail: oelsayed@uwm.edu

Ryoichi S. Amano
Professor
Fellow ASME
Department of Mechanical Engineering,
University of Wisconsin—Milwaukee,
Milwaukee, WI 53211
e-mail: amano@uwm.edu

J. R. Strickler
Professor
Department of Biological Sciences,
University of Wisconsin—Milwaukee,
Milwaukee, WI 53204
e-mail: Strlab1@uwm.edu

P. Hinow
Professor
Department of Mathematical Sciences,
University of Wisconsin—Milwaukee,
Milwaukee, WI 53201
e-mail: hinow@uwm.edu

Houshuo Jiang
Department of Applied Ocean Physics and Engineering,
Woods Hole Oceanographic Institution,
Woods Hole, MA 02543
e-mail: hsjiang@whoi.edu

Paul C. Sikkel
Professor
Department of Biological Sciences,
Arkansan State University,
Jonesboro, AR 72401
e-mail: psikkel@astate.edu

N. Kohls
Department of Mechanical Engineering,
University of Wisconsin—Milwaukee,
Milwaukee, WI 53211
e-mail: ndkohls@uwm.edu

Mass Transfer Performance of a Marine Zooplankton Olfactometer

By adopting different methods to the inlet of a zooplankton olfactometer, the current study investigates the effect of the energy of chemical flow on the Gnathiid isopod crustaceans predicted behavior. These are mobile external parasites of fishes that have a significant impact on the health of their hosts. They rely at least in part on olfactory cues to find the host fish. To better understand host-finding dynamics in these parasites, a study was conducted with the simulations as a blueprint for developing a 3-dimensional test apparatus similar to what has been used for studying olfactory orientation in insects. The simulated olfactometer has four legs, each leg forming an inlet where fluids are introduced into the flow domain. There is one outlet at the center of the device. A mixture of water and chemicals is presented by applying a multi-component system. The shear and chemical concentration distribution were conducted to see how fluid physics plays a role in creating a chemical landscape. Computational results show distinct regions separated by high chemical concentration gradients when introducing chemicals from one leg. Changing the fluid inflow from one common inlet to three inlets shows that the chemical distribution exhibits steeper gradients than the typical inlet case, depicting that the gradual chemical concentrations can drive the animal toward the target faster. The best behavior that gives higher chemical gradients is obtained through the study when using three sub-inlets and Schmidt number between 3 and 10. [DOI: 10.1115/1.4049602]

Keywords: mass and energy transfer, computational fluid dynamics, zooplankton behavior, chemical sensing

1 Introduction

All aquatic organisms live in a chemical environment and rely on chemical cues in that environment during at least some aspect of their life cycles [1,2]. Chemical signals can be used for multiple essential functions, including mate attraction [3,4], location of habitat [5,6], and food [7,8], as well as an escape from enemies [9,10]. Thus, an understanding of aquatic communities requires an understanding of their chemical environment and how they respond to and utilize chemical cues [11].

Chemical ecology, the science of chemical signals produced and utilized by organisms, and how those cues affect ecologically relevant responses [1,12] has focused on determining chemical cue structure, the information contained in those cues, and the behaviors elicited when the cues are encountered [13,14]. An olfactometer is

Contributed by the Advanced Energy Systems Division of ASME for publication in the Journal of Energy Resources Technology. Manuscript received December 5, 2020; final manuscript received January 2, 2021; published online February 3, 2021. Editor: Hameed Metghalchi.

an instrument that creates a known, sectioned chemical landscape and allows the observation of animals that behave within this landscape. When a significant majority of test animals frequented one section of the landscape, one infers that they perceived this section's smell and preferred it to all the other sections. In aquatic systems, the standard olfactometer used for smaller organisms has been the y-maze [15,16]. However, this approach has limitations in that it does not effectively replicate the complex, 3-dimensional chemical environment aquatic organisms must navigate.

To test olfaction in Leptopilina clavipes, a parasitoid wasp, Vet et al. [17] developed an airflow olfactometer. Four quarter sections stemming from a 1 cm ring cut from a Perspex tubing of a diameter of 270 mm were glued on a Perspex sheet of 200×200 mm to form a star shape arena. Each corner of the star is an inlet of conditioned air flowing at equal speed into the arena. At the center of the arena was an outlet for the flow stemming from the four inlets. The arena was covered, and one animal at a time was released in the center of it. Video-recording allowed analyses of the behaviors of the animals.

The flow from the four corners of the arena creates four distinct, contiguous odor fields that the test animal can enter at will, leave, re-enter, and finally end up at one of the odor entries. In this way, one can test three different smells versus control or two other compounds and a mixture of the two versus a control. Changing the setting helps figure out the minute details of what compound or a mixture of compounds are the most effective triggering behavior in the animal. To verify that the four odor fields are separated from each other and only meet at stable, sharp boundaries, they visualized the chemical landscape by adding smoke to the air.

To date, 362 published peer-reviewed contributions cite the seminal paper of Vet et al. [17]. Most of them show results from testing terrestrial parasitoids finding their hosts, food, and mates. For example, some species of ground beetles find weed seeds. Results show that imbibed Brassica napus seeds were preferred over other weed species by two of the three carabid species tested [18]. Similarly, Goldman-Huertas et al. [19] tested herbivorous flies (*Scaptomyza flava*; Drosophilidae) and found that they differ in their reaction to yeast-associated volatiles from the reactions of *Drosophila melanogaster*. This result led them to compare the odorant receptor repertoires of the two species ending in the conclusion that major trophic shifts in insects are associated with chemoreceptor gene loss. An overview of the current thinking about the challenges in the neurobiology of insect olfaction can be found in Martin et al. [20]. To have four, as in Vet et al. [17], or six, as in Turlings et al. [21], distinct sections with sharp boundaries that do not vacillate, one needs to have a low Reynolds number environment creating and maintaining steady flow.

Many "insect-like" marine invertebrates similarly rely heavily on olfactory cues. These are external parasites with highly mobile "zooplankton" stages that must locate and then swim to a host to complete their life cycle. Among the most common of these are parasitic crustaceans such as gnathiid isopods [18], which rely at least in part on olfactory cues to locate their fish hosts [22,23]. As the next step toward advancing the understanding of chemotaxis in small marine organisms, we aim to adapt the apparatus developed by Vet et al. [17] for use in aquatic systems, using gnathiid isopods as "model" test organisms.

The working medium for marine organisms is water, while for the olfactometer is air. For the same temperature, because the water is 50 times as viscous as air and roughly 830 times as dense, its kinematic viscosity is smaller than that of air by a factor of 8 to 15. Consequently, an object of a given characteristic length moving at a given speed has a Reynolds number 8- to 15-fold larger in water than in air. The same device filled with water may then tend toward turbulent flow while at the same speed of delivery, destroying the distinct chemical landscape. The experimental results exhibit flow instability associated with the turbulence nature in the observations even in very low-Reynolds number cases. Such phenomena were eye-witnessed by many researchers such as Tsukahara et al. [24] and Fukudome et al. [25] for the Reynolds number as low as 60 and Ghalichi et al. [26] with Reynolds number less than 400.

To validate our model, the authors conduct a series of computational fluid dynamics (CFD) simulations using the water flow geometry and flow parameters and compared them with Vet et al. [17]. To predict gnathiid isopod behavior, we consider the velocity profile, the shear stress, and the chemical landscape's effect as the animal moves within the flow field. Therefore, the current study helps understand the proper experimental method to predict the response of these species by using different design conditions that a specific chemical distribution, which depends on the fluid energy [27–31], can stimulate their olfaction behavior.

2 Methodology

2.1 Flow Domain. In this study, we use computer simulations to model the effects of different factors on the animal's behavior. All CFD simulations were conducted based on a model for marine zooplankton olfaction. The flow domain is similar to the one used by Vet et al. [17] in their experimental work. As shown in Fig. 1, water flows from four inlet arms toward the center outlet. All inlets and the outlet have the same diameter of 10 mm. When using water instead of air, the shear Reynolds number is set to $\mathrm{Re} = 50$ to match the flow conditions. Air or water can be used as long as the Reynolds number is the same, but since this is a marine application, most of the simulations are conducted with water as the flowing fluid.

2.2 Governing Equations. The continuity and momentum equations are first solved to obtain the fluid flow behavior, and then depending on the case considered, additional equations are required to solve. We refer to Ref. [32] for more background on mass transport phenomena. In several CFD simulations, the momentum equation is solved separately for each velocity component in a 3D representation. Subsequently, the pressure is corrected based on the continuity equation. Figures 2 and 3 show the velocity profile for each of the air and water flow.

The mass fractions of the species used were obtained by using a multi-component model, where the gas or liquid mixture consists of more than one component. Diffusion occurs due to concentration gradients of the components of the mixture [33]. We use the software package Star-CCM [34] to predict the local mass fraction of each species, *Yi*, by solving a convection-diffusion equation

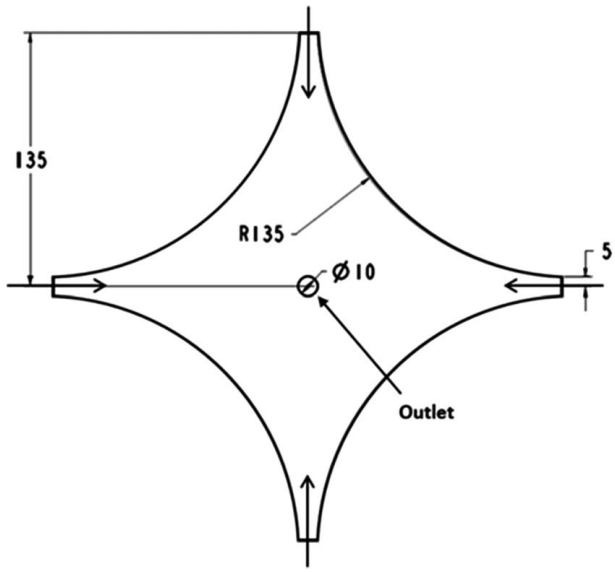

Fig. 1 The marine zooplankton test section with four inlets and one outlet

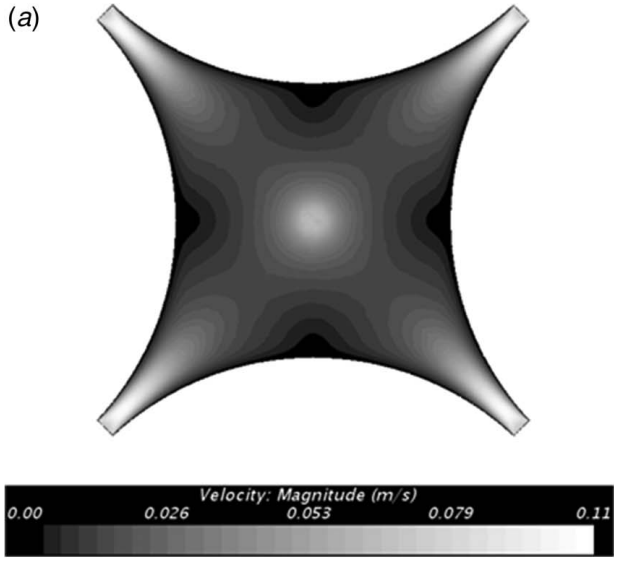

Fig. 2 Velocity magnitude color contours of air (*a*), with a flowrate of 4 × 0.3 l/min, and of water (*b*), with a flowrate of 4 × 0.02 l/min. The shear Reynolds number in both cases is Re = 50.

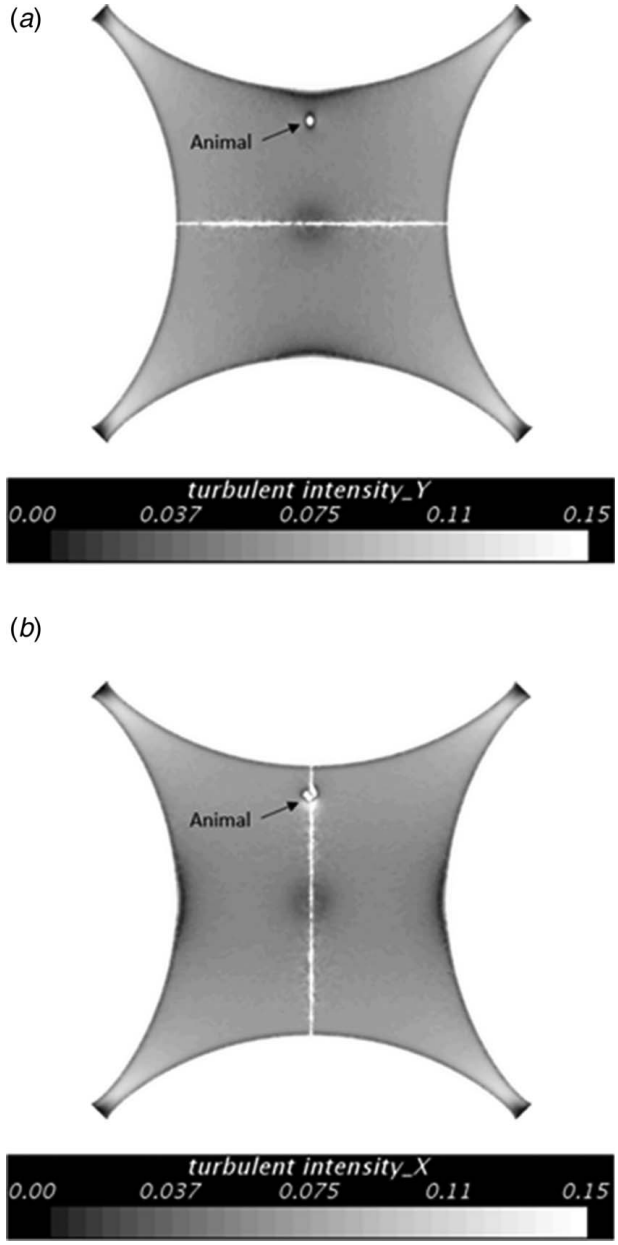

Fig. 3 Turbulent intensity: (*a*) *X*-direction and (*b*) *Y*-direction

[35,36]. This conservation equation takes the following form:

$$\frac{\partial Y_i}{\partial t} + \nabla \cdot (\mathbf{v} Y_i) = \left(\frac{\nu_i}{Sc_i} + \frac{\mu_t}{\rho Sc_t} \right) \nabla^2 Y_i + R_i \tag{1}$$

Equation (1) is applied unsteady, turbulent flow, and fluid properties are constant. The mixtures (water or air + chemical) are not reacting. Therefore the rate of production of species i (R_i) is equal to zero.

Different Schmidt numbers up to 500 are considered in this study. To find the velocity field, we solve the momentum equation [37]:

$$\frac{\partial}{\partial t}(\rho \mathbf{v}) + \nabla \cdot (\rho \mathbf{v}\mathbf{v}) = -\nabla p + \nabla \cdot (\mu \nabla \mathbf{v} + \tau_t) \tag{2}$$

Equation (2) can be called the general momentum equation since it accounts for instability and turbulence.

2.3 Boundary and Internal Flow Conditions. For most of the cases discussed here, the boundary conditions are a constant velocity at all the four inlets, while atmospheric pressure is applied at the center outlet. We have observed low-Reynolds number turbulence behavior in the experimental results. Therefore, the turbulence intensity was produced by using the large eddy simulation (LES), as shown in Fig. 3, which is different from the Reynolds-averaged Navier–Stokes (RANS) solver. When using the LES simulation technique, turbulent energy with length scales up to grid sizes is directly resolved, and the rest is treated adopting hybrid-LES/RANS [38–40]. Therefore, this technique requires a finer mesh than other so-called "turbulent models." The calculation of turbulence intensity was aimed to show the significance of turbulence. From these results, it is demonstrated that turbulence occurs at regions near the inlets of the flow domain, while most of the domain exhibits low turbulence. This trend is mainly due to a high shear-flow appearing at the inlet regions, attributed to hydroinstability. The experimental observation also confirmed these phenomena in the literature. This flow behavior shows that the laminar assumption is valid.

The mass fraction of each component is specified at the boundaries of the flow domain, where the chemical enters the flow field

from one or all of the legs. In some of the cases discussed here, the mixture of chemical and water is entering from one or more inlets while water or air enters the rest of the inlets except for the case with three sub-inlets, as it will be shown later, each fluid enters separately. For this case, the mixture status does not apply at the inlet. This means all fluid components are entering as substances, not mixtures.

2.4 Mesh Independent Test. Mesh independency test is conducted by considering three cases; 250k, 500k, and 1M mesh cells. This test was performed based on the chemical concentration versus mesh cells number at a plane on the median distance between the inlet and outlet, as shown in Fig. 4 and Table 1. The mesh independence shows that the chemical concentration at the selected region is changing very slightly, which can be shown that it is constant, and therefore, 250k mesh cells are sufficient to use for obtaining all the results required for the current work.

3 Results and Discussions

3.1 Chemical-Air Admittance From Four Outlets. The CFD results of the mass fraction of the chemical-air mixture are compared with the experimental results obtained by Vet et al. [17]. These results are helpful to distinguish the physics effect from the chemistry effect on animal behavior.

Figure 5 shows the CFD results of the mass fraction of the chemical at different physical times. These are obtained for the purpose of comparisons with the experimental measurements of the air-chemical photos from Vet et al. [17]. The compassion shows an acceptable agreement with the experimental measurements. Though, Vet results show nonuniformities opposite to the CFD results. This is due to the ideal conditions assumed by the CFD results, which ignore any friction or nonuniformities in the flow conditions. This is very important in this case because CFD will limit any effect other than the impact of physics and chemistry. Therefore, this is another reason to get benefits from the CFD approach.

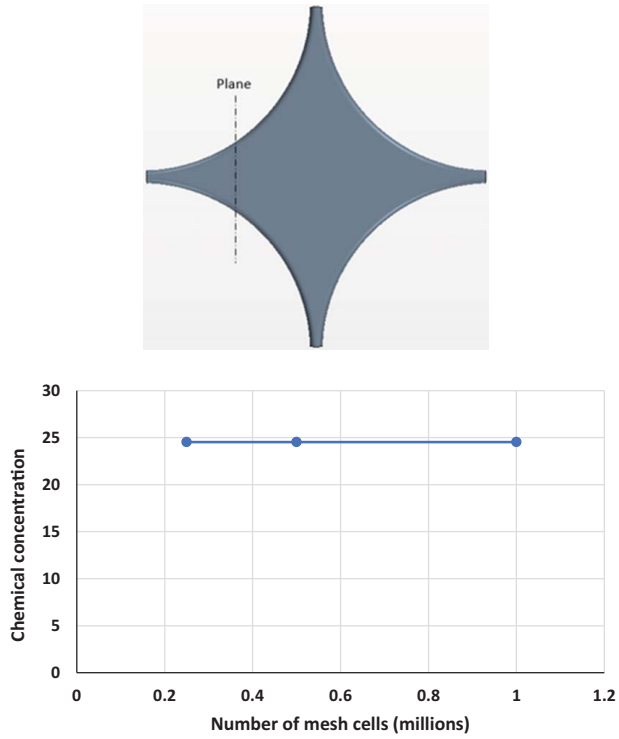

Fig. 4 Mesh independency

Table 1 Mesh independency

Number of mesh cells (millions)	Chemical concentration
0.25	24.534
0.5	24.531
1	24.528

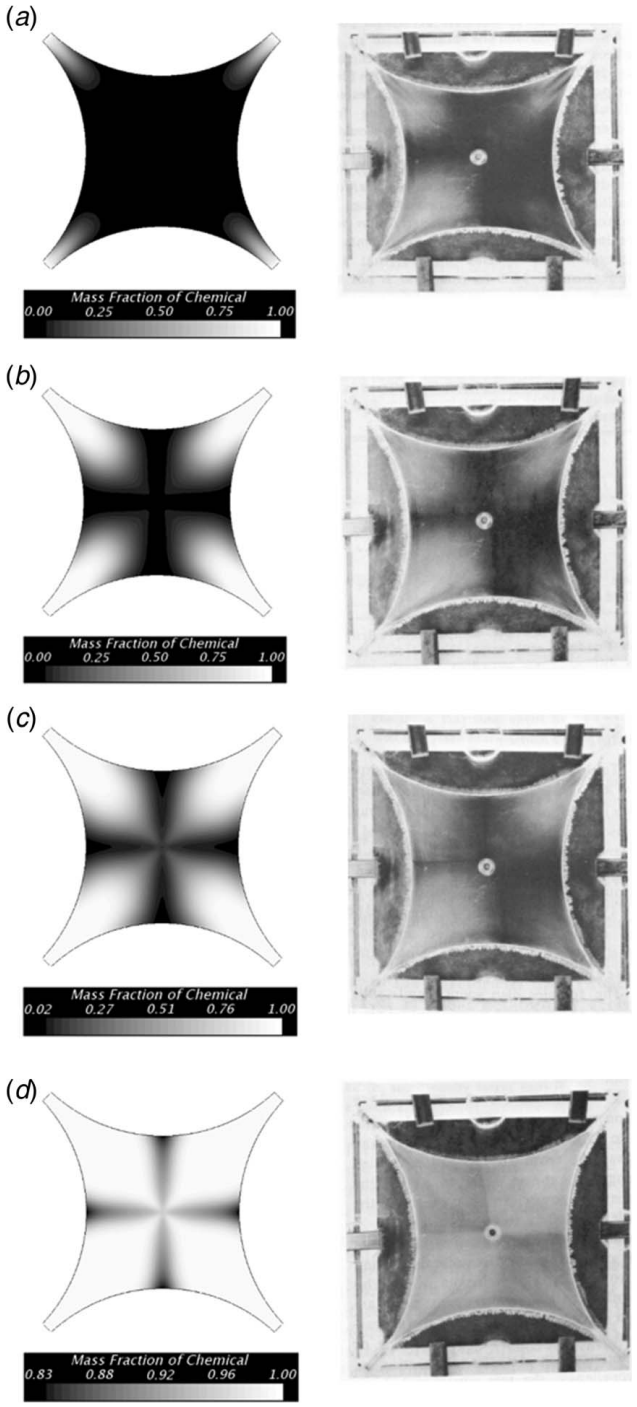

Fig. 5 Mass fraction of the chemical at different physical times; results on the left are CFD: (*a*) 0.5 s, (*b*) 4 s, (*c*) 6 s, and (*d*) 24 s; results on the right are experimental adapted from Vet et al. [17]

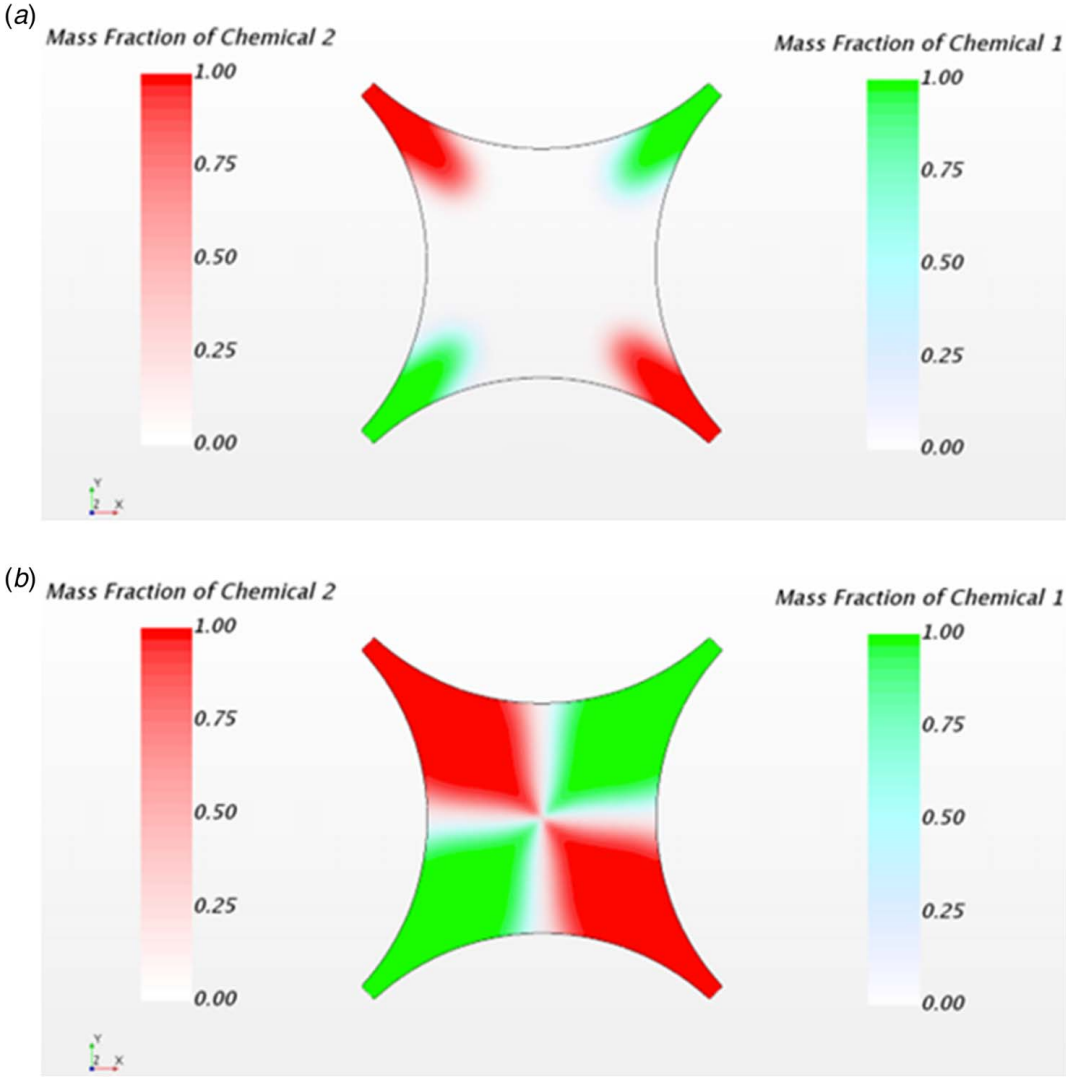

Fig. 6 Mass fraction of chemicals when two chemicals flow from opposite inlets toward the outlet: (*a*) $t = 3$ s and (*b*) $t = 12$ s

3.2 Investigating Multiple Chemicals. Commonly, pheromones and kairomones are mixtures of multiple chemical compounds. These may have different diffusion rates, decay rates, or they may be involved in chemical reactions among each other.

Figure 6 shows the mass fraction of two different compounds at different times t. Each compound is introduced from two opposing inlet legs. All substances are entering as a mixture of two components (chemical and air or water).

3.3 Shear Stress. When the animal moves in the observation domain, it takes a path that has both deterministic and random components. The deterministic component could be influenced by factors such as shear stress and chemical gradients.

Figure 7 shows the shear stress exerted by the fluid on the animal as it moves to start from the center outlet toward the inlet or the chemical source. This shows higher shear stress in two regions; close to the outlet and close to the inlet. It is normal in these regions to see higher shear stress because of the higher velocity gradients caused by the area contraction. Therefore, the animal is forced to exist in these regions. For the rest region, the animal is taking a more natural path represented by low shear stress.

3.4 Case With Three Sub-Inlets. The way by which the chemical is introduced into the flow domain can influence the location and spatial variation of the chemical gradient. The purpose is to generate a gradual chemical gradient that goes across space between the source inlet and the outlet. By following this gradual chemical gradient, the animal's olfactory behavior can allow the animal to distinguish the favorable and unfavorable regions, thereby attracting the animal toward the targeted source, e.g., one of the four inlet legs.

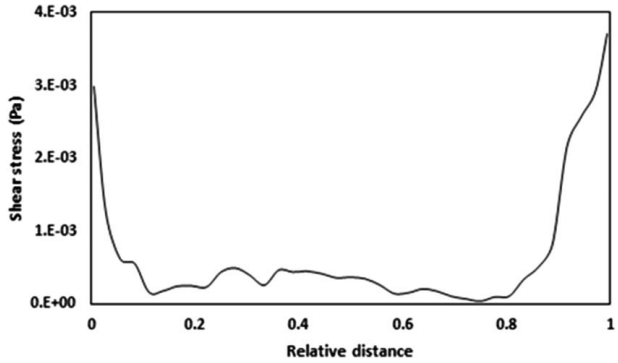

Fig. 7 Shear stress along the animal walking track experimented by Vet et al. [17]

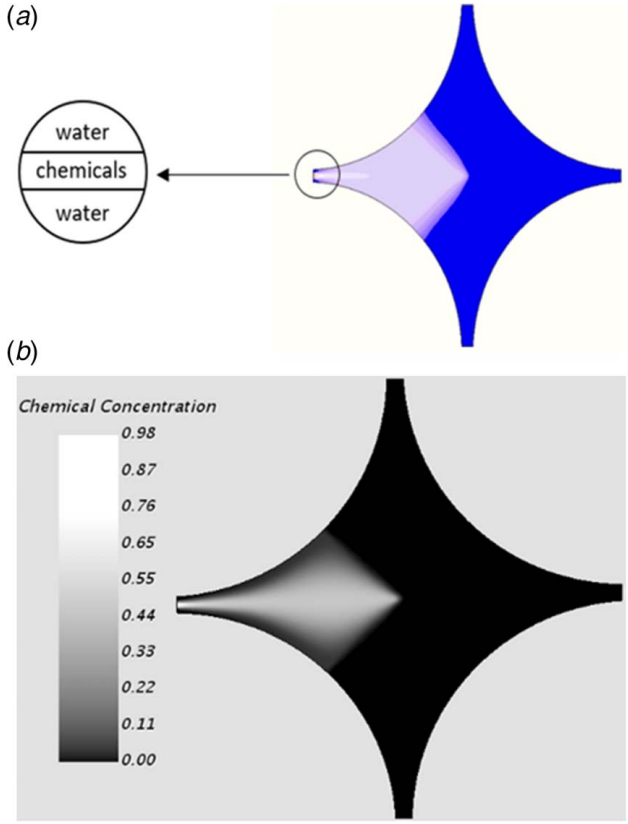

Fig. 8 Chemical concentration for the case with three sub-inlets: (*a*) color scale and (*b*) grayscale

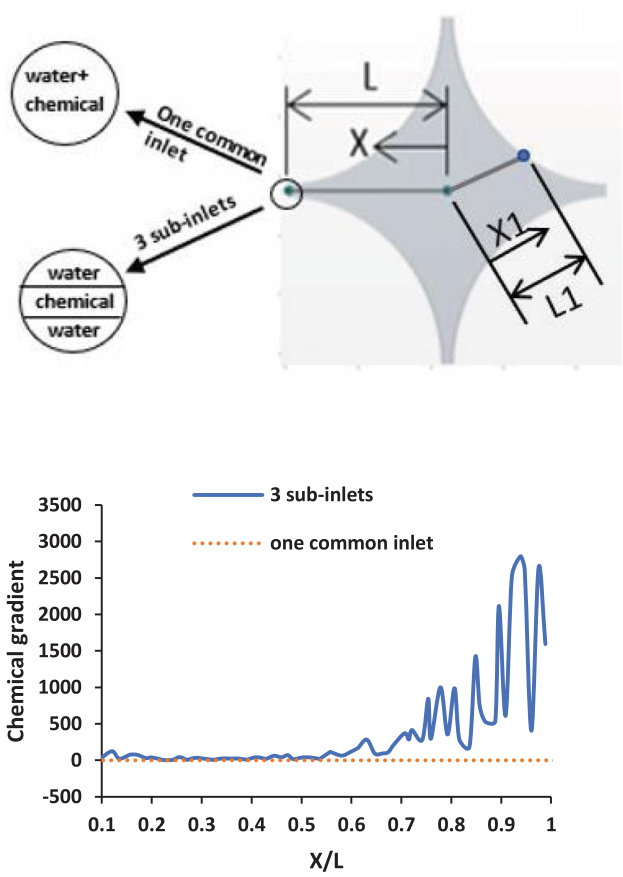

Fig. 9 Chemical gradient for one common inlet versus three sub-inlets

For the case with three sub-inlets, only water is used as the working fluid with one of the inlet legs subdivided into three sub-inlets, as shown in Fig. 8. Because a sharp chemical gradient is introduced right at the inlet surface, the chemical gradient is forced to vary gradually from the inlet surface to the outlet, thereby forming a desired, gradually varying, chemical gradient along the central path of the flow domain. This is different from the case of using one common inlet to introduce water and chemicals together, for which there is no variation in the chemical gradient (Fig. 9). The setup with three sub-inlets is more interesting since it can more readily induce the animal's olfactory behavior by creating a gradually varying chemical gradient across the flow domain.

The case with three sub-inlets has shown a promising development in creating a variable chemical distribution. Therefore, further investigation by applying the CFD approach to expand the outcome of this design can be potentially useful.

Figures 10(*a*) and 10(*b*) shows the chemical concentration along two lines; one line is plotted from the outlet to the three sub-inlet sections, and the other one is plotted to the right side wall as shown in Fig. 9. The effect of Schmidt number (Sc) on the chemical concentration was investigated, as shown in Figs. 10(*a*) and 10(*b*). It is noted from Fig. 10(*a*) as Sc increases, the chemical concentration increases too, but this increase takes a similar gradient for all the Schmidt numbers considered in this case. On the other hand, Fig. 10(*b*) shows as Sc decreases, the behavior of the chemical concentration tends to be constant (the chemical distributes evenly across the flow domain). This is attributed to the increase in diffusion when decreasing the Schmidt number, which decreases the momentum required by the chemical to diffuse in water. Also, when increasing the Schmidt number beyond 100, there will be no significant chemical concentration changes. Based on these results, the higher gradients' best behavior can be considered when the Schmidt number ranges between 3 and 10.

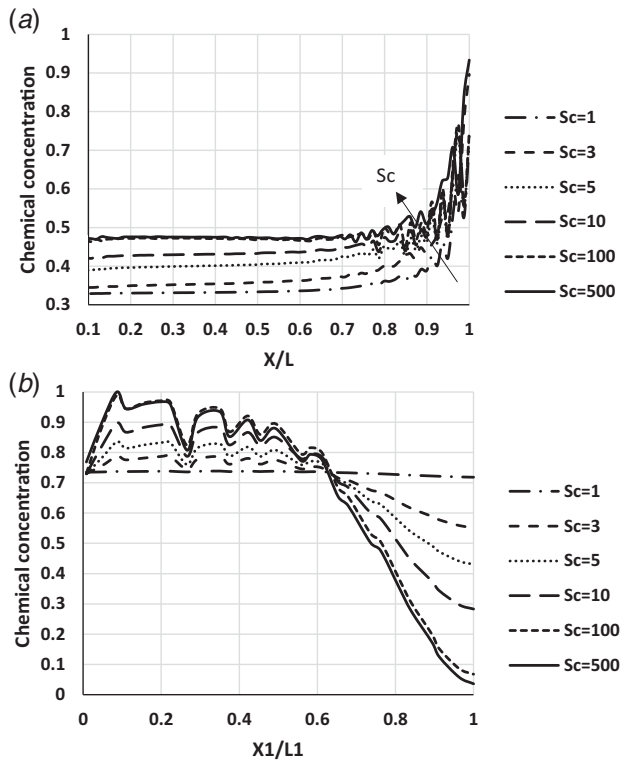

Fig. 10 Chemical concentrations at different Schmidt numbers (Sc): (*a*) along *X*/*L* and (*b*) along *X*1/*L*1

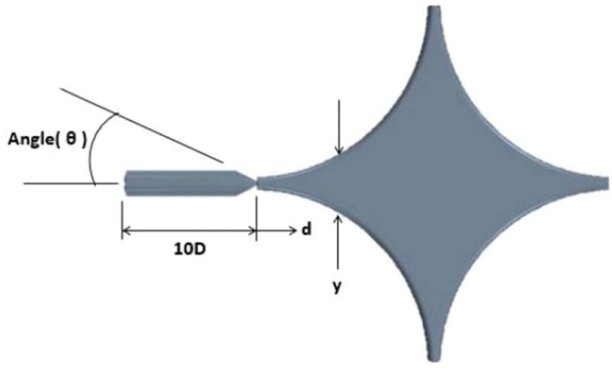

Fig. 11 CFD model for the entry nozzle setup

3.5 Effect of Entry Profile. In this part, a comparison between different convergent nozzles is conducted. Based on the nozzle angle, the inlet velocity profile effect on the diffusion of chemicals in the water-chemical domain was investigated.

Figure 11 shows the setup of a nozzle with an angle θ at the left leg. The flow enters the nozzle from the left side and exits the nozzle to enter the flow domain.

Three cases were considered depending on three nozzle angles θ, i.e., 0, 13, and 26 deg. Also, the nozzle length is equal to $10D$, corresponding to the entrance length for a low Reynolds number flow according to (3):

$$\frac{\text{Le}}{D} = 0.06\text{Re}_D \tag{3}$$

Figures 12 shows the chemical concentration profile for each angle at a different distance (d), which is measured from the edge of the left leg of the flow domain. These profiles show a higher concentration at a lower d and a lower concentration at a higher d. This behavior is reasonable since the area near the edge is small (higher velocity) compared with the area downstream. Also, it is noted from these results that a slightly higher concentration can be obtained when $\theta = 26$ deg than when $\theta = 13$ deg while the lowest concentration can be seen when $\theta = 0$ deg.

A similar way is used to obtain Fig. 13, where the kinetic energy of chemical was obtained for different (d). The kinetic energy

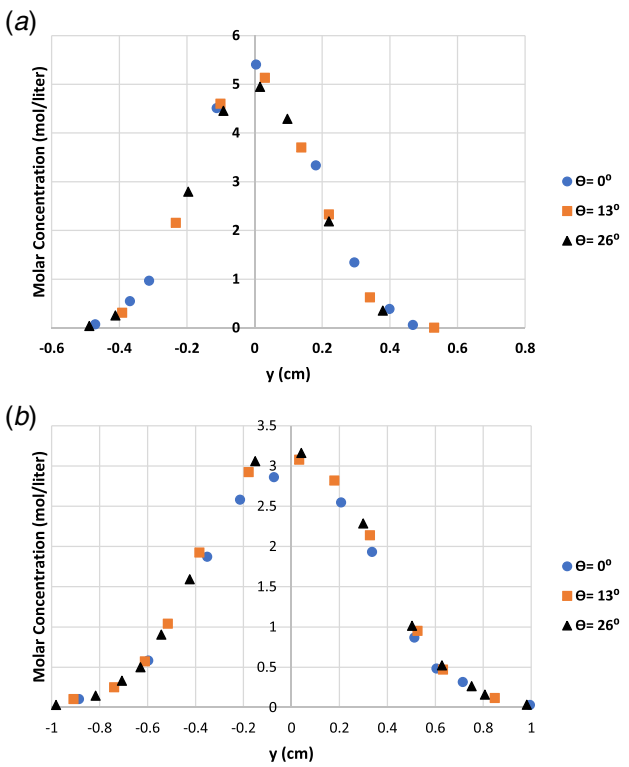

Fig. 12 Molar concentration of chemical when (*a*) $d = 2$ cm, (*b*) $d = 4$ cm, (c) $d = 6$ cm, and (*d*) $d = 8$ cm

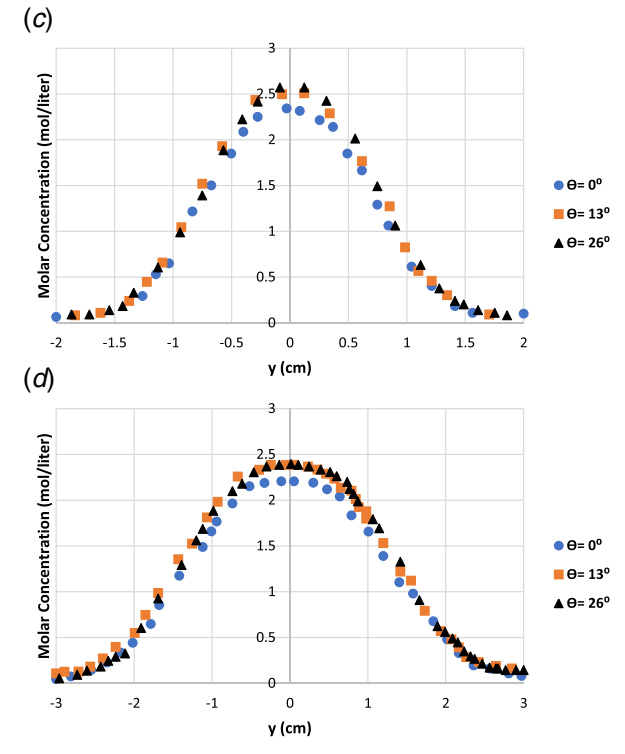

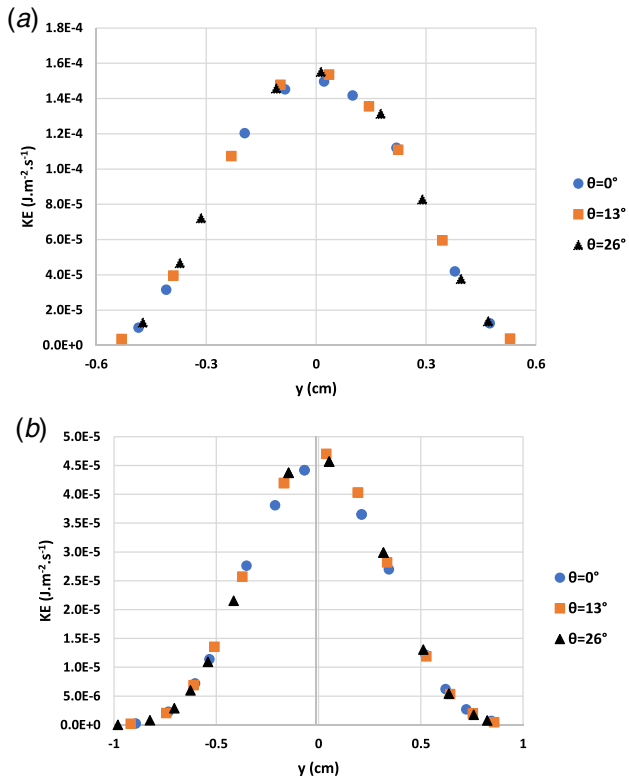

Fig. 13 Kinetic energy of chemical when (*a*) $d = 2$ cm, (*b*) $d = 4$ cm, (c) $d = 6$ cm, and (*d*) $d = 8$ cm

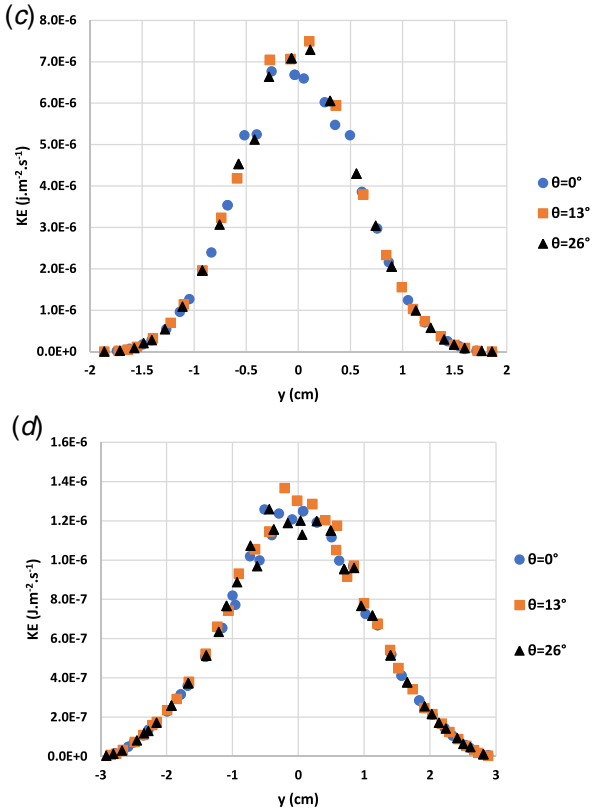

seems to follow close behavior to the results of Fig. 12 for the chemical concentration. It can be seen that as the distance (d) increases (approaching the outlet), the kinetic energy decreases. Also, it can be seen from Fig. 13, for all the cases, the kinetic energy is higher for the 13 and 26 deg than the 0 deg.

4 Conclusions

This study aimed to estimate the olfactory response of fish-parasitic gnathiid isopods by introducing an olfactometer based on CFD. From the results, it can be first inferred that under the flow conditions used for this study, the flow is not influenced by any significant disturbance to affect the animal's behavior. This leads one to conclude that a chemical map is the most significant factor to drive the animal's olfaction response.

It is more favorable in terms of the animal's olfaction behavior to consider some of the factors to create chemical concentration gradients, such as using three sub-inlets instead of one standard inlet or introduce the flow to the domain by using a convergent nozzle with high convergence angle where the need for a steep concentration could be necessary to "drag" the animal toward a specific region.

Finally, it was discovered that, as Sc increases, the chemical concentration become strongly dependent on the location. However, as Sc decreases, the behavior of the chemical concentration tends to be constant (chemical distributes evenly across the flow domain). This is attributed to the increase in diffusion when decreasing the Schmidt number, which decrease the momentum required by the chemical to diffuse in water. The trend of the kinetic energy is in accordance to the chemical concentration, and the magnitude of the kinetic energy depends on the nozzle entrance angle.

Acknowledgment

The research is funded by the University of Wisconsin-Milwaukee, RGI grant.

Conflict of Interest

There are no conflicts of interest.

Data Availability Statement

The datasets generated and supporting the findings of this article are obtainable from the corresponding author upon reasonable request. The authors attest that all data for this study are included in the paper. Data provided by a third party listed in Acknowledgment. No data, models, or code were generated or used for this paper.

Nomenclature

d = distance measured from the leg inlet
t = time
y = distance between two adjacent walls
A = area
D = diameter of the entrance nozzle
P = pressure
V = volume
Y = mass fraction
S_i = source term accounts for reacting components
Le = entrance length
Re = shear Reynolds number at the olfactometer inlet
Sc = Schmidt number
Sc_t = turbulent Schmidt number
$\boldsymbol{\upsilon}$ = velocity field

Greek Symbols

θ = entry nozzle angle
μ = dynamic viscosity
μ_t = turbulent viscosity
ν = kinematic viscosity
ρ = density
τ_t = turbulent shear stress

References

[1] Eisner, T., and Meinwald, J., 1995, "Chemical Ecology," Proc. Natl. Acad. Sci. USA, **92**(1), p. 1.
[2] Penn, D. J., 2006, "Chemical Communication: Five Major Challenges in Post-Genomic Age," *Chemical Ecology: From Gene to Ecosystem*, M. Dicke, and W. Takken, eds., Springer-Verlag, pp. 9–18,
[3] Lonsadale, D. J., Frey, M. A., and Snell, T. W., 1998, "The Role of Chemical Signals in Copepod Reproduction," J. Mar. Syst., **15**(1–4), pp. 1–12.
[4] Sanders, K. M., Brockmann, H. J., Watson W. H. III, and, Jury, S. H., 2010, "Male Horseshoe Crabs Limulus Polyphemus Use Multiple Sensory Cues to Locate Mates," Curr. Zool., **56**(5), pp. 485–498.
[5] Pawlik, J. R., 1992, "Chemical Ecology of the Settlement of Benthic Marine Invertebrates," Oceanogr. Mar. Biol. Annu Rev., **30**, pp. 273–335.
[6] Dixson, D. L., Abrego, D., and Hay, M. E., 2014, "Chemically Mediated Behavior of Recruiting Corals and Fishes: A Tipping Point That May Limit Reef Recovery," Science, **345**(6199), pp. 892–897.
[7] Derby, C. D., Steullet, P., Horner, A. J., and Cate, H. S., 2001, "The Sensory Basis of Feeding Behavior in the Caribbean Spiny Lobster, Panulirus Argus," Mar. Freshwater Res., **52**(8), pp. 1339–1350.
[8] Keller, T. A., Tomba, A. M., and Moore, P. A., 2001, "Orientation in Complex Chemical Landscapes: Spatial Arrangement of Chemical Sources Influences Crayfish Food-Finding Efficiency in Artificial Stream," Limnol. Oceanogr., **46**(2), pp. 238–247.
[9] Chivers, D. P., Brown, G. E., and Smith, R. J. F., 1995, "Acquired Recognition of Chemical Stimuli From Pike, Esox Lucius, by Brook Sticklebacks, *Culaea inconstans* (Osteichthyes, Gasterosteidae)," Ethology, **99**(3), pp. 234–242.
[10] Gazdewich, K. J., and Chivers, D. P., 2002, "Acquired Predator Recognition by Fathead Minnows: Influence of Habitat Characteristics on Survival," J. Chem. Ecol., **28**(2), pp. 439–445.
[11] Dicke, M., and Takken, W., 2006, *Chemical Ecology: A Multidisciplinary Approach*, Chemical Ecology: From Gene to Ecosystem, Springer, The Netherlands, 2006, pp. 1–8.
[12] Rajagopalan, K., and Nihous, G. C., 2013, "An Assessment of Global Ocean Thermal Energy Conversion Resources With a High-Resolution Ocean General Circulation Model," ASME J. Energy Resour. Technol., **135**(4), p. 041202.

[13] Westermann, B., and Beuerlein, K., 2005, "Y-maze Experiments on the Chemotactic Behavior of the Tetrabranchiate Cephalopod *Nautilus pompilius* (Mollusca)," Mar. Biol., **147**(1), pp. 145–151.
[14] Seepersad, B., Ramnath, K., Dyal, S., and Mohammed, R., 2004, "The Use of Aniline Blue for the Determination of Dead Phytoplankton, Zooplankton and Meroplankton in LC 50 Testing After 96h… A Re-Evaluation of the US Environmental Protection Agency Methodology," ASME J. Energy Resour. Technol., **126**(3), pp. 215–218.
[15] Zheng, S., and Yang, D., 2017, "Experimental and Theoretical Determination of Diffusion Coefficients of CO_2 -Heavy Oil Systems by Coupling Heat and Mass Transfer," ASME J. Energy Resour. Technol., **139**(2), p. 022901.
[16] Wang, H., Vedapuri, D., Cai, J. Y., Hong, T., and Jepson, W. P., 2001, "Mass Transfer Coefficient Measurement in Water/Oil/Gas Multiphase Flow," ASME J. Energy Resour. Technol., **123**(2), pp. 144–149.
[17] Vet, L., Lenteren, J. C. V., Heymans, M., and Meelis, E., 1983, "An Airflow Olfactometer for Measuring Olfactory Responses of Hymenopterous Parasitoids and Other Small Insects," Physiol. Entomol., **8**(1), pp. 97–106.
[18] Kulkarni, S., Dosdall, L., Spense, J., and Willenborg, C., 2017, "Seed Detection and Discrimination by Ground Beetles (Coleopetra: Carabidae) Are Associated With Olfactory Cues,? PLoS ONE, **12**(1), p. e0170593.
[19] Goldman-Huertas, B., Mitchell, R., Lapoint, R., Faucher, C., Hilderbrand, J., and Whiteman, N., 2015, "Evolution of Herbivory in Drosophilidae Linked to Loss of Behaviors, Antennal Responses, Odorant Receptors, and Ancestral Diet, " Proc. Natl. Acad. Sci., **112**(10), pp. 3026–3031.
[20] Martin, J., Beyerlein, A., Dacks, A., Resenman, C., Riffell, J., Lei, H., and Hildebrand, J., 2011, "The Neurobiology of Insect Olfaction: Sensory Processing in a Comparative Context," Progress Neurol., **95**(3), pp. 427–447.
[21] Turlings, T., Tamo, C., and Davidson, A., 2004, "A Six-Arm Olfactometer Permitting Simultaneous Observation of Insect Attraction and Odour Trapping," Physiol. Entomol., **29**(1), pp. 45–55.
[22] Sikkel, P. C., and Welicky, R. L., 2019, *State of Knowledge and Future Trends*, N. J. Smit, N. L. Bruce, and K. A. Hadfeld, eds., Springer International Publishing, Springer Nature, Switzerland, pp. 421–477.
[23] Sikkel, P. C., Sears, W. T., Weldon, B., and Tuttle, B. C., 2011, "An Experimental Field Test of Host-Finding Mechanisms in a Caribbean Gnathiid Isopod," Mar. Biol., **158**(5), pp. 1075–1083.
[24] Tsukahara, T., Seki, Y., Kawamura, H., and Tochio, D., 16 Sep 2014, "DNS of Turbulent Channel Flow at Very Low Reynolds Numbers," Proceedings of Turbulence and Shear Flow Phenomena Conference., Williamsburg, VA.
[25] Fukudome, K., Lida, O., and Nagano, Y., "The Mechanism of Energy Transfer in Turbulent Poiseuille Flow at Very Low-Reynolds Number," Sixth International Symposium on Turbulence and Shear Flow Phenomena Seoul, South Korea, June 22–24, 2009.
[26] Ghalichi, F., Deng, X., De Champlain, A., Douville, Y., King, M., and Guidoin, R., 1998, "Low Reynolds Number Turbulence Modeling of Blood Flow in Arterial Stenosis," Biorheology, **35**(4,5), pp. 281–294.
[27] Hasan, A., and Dincer, I., 2019, "A New Integrated Ocean Thermal Energy Conversion-Based Trigeneration System for Sustainable Communities," ASME J. Energy Resour. Technol., **142**(6), p. 061301.
[28] Nihous, G. C., 2007, "A Preliminary Assessment of Ocean Thermal Energy Conversion Resources," ASME J. Energy Resour. Technol., **129**(1), pp. 10–17.
[29] Nihous, G. C., 2005, "An Order-of-Magnitude Estimate of Ocean Thermal Energy Conversion Resources," ASME J. Energy Resour. Technol., **127**(4), pp. 328–333.
[30] Shashaty, A. J., 1983, "Nonlinear and Hysteretic Twisting Effects in Ocean Cable Laying," ASME J. Energy Resour. Technol., **105**(3), pp. 341–345.
[31] Chung, J. S., and Felippa, C. A., 1981, "Nonlinear Static Analysis of Deep Ocean Mining Pipe-Part II: Numerical Studies," ASME J. Energy Resour. Technol., **103**(1), pp. 16–25.
[32] Sherwood, T., Pigford, R., and Wilke, C., 1975, *Mass Transfer*, McGraw-Hill Chemical Engineering Series, New York.
[33] Woodford, O. SC—Powerful Image Rendering. https://www.github.com/ojwoodford/sc, GitHub. Accessed January 8, 2020.
[34] C.D-adapco, 2016, *STAR-CCM+ 11.0 User Guide*, CD-adapco Inc., Melville, NY.
[35] Lee, Y. E., and Li, S. F. Y., 1991, "Binary Diffusion Coefficients of the Methanol/Water System in the Temperature Range 30-40 Degree.C," J. Chem. Eng. Data, **36**(2), pp. 240–243.
[36] Karim, G. A., Lam, H. T., Petela, R., and Rowe, R., 1987, "Experimental and Analytical Investigation of the Convective Diffusion of Methane Into Air," ASME J. Energy Resour. Technol., **109**(4), pp. 230–234.
[37] Sohrab, S. H., 2014, "Invariant Forms of Conservation Equations and Some Examples of Their Exact Solutions," ASME J. Energy Resour. Technol., **136**(3), p. 032002.
[38] Shen, H., Zhang, Y., Wu, Y., Zhou, M., Zhang, H., and Yue, G., 2020, "Modeling of the Coal Particle Behavior in an Ultra-Supercritical Boiler With Large Eddy Simulation," ASME J. Energy Resour. Technol., **142**(7), p. 070909.
[39] Selim, O. M., Elgammal, T., and Amano, R. S., 2020, "Experimental and Numerical Study on the Use of Guide Vanes in the Dilution Zone," ASME J. Energy Resour. Technol., **142**(8), p. 083001.
[40] Jain, S., and Saha, U. K., 2020, "Capturing the Dynamic Stall in H-Type Darrieus Wind Turbines Using Different URANS Turbulence Models," ASME J. Energy Resour. Technol., **142**(9), p. 091302.